DOI: 10.13009/EUCASS2022-6140
9TH EUROPEAN CONFERENCE FOR AERONAUTICS AND SPACE SCIENCES (EUCASS)

Analysis and Design of Unmanned Aerial Systems for Precision Agriculture applications on Vineyards

Nicoletta Bloise[⋆]*, Manuel Carreño Ruiz*[⋆†]*, Erika Mai*[♮]*, Domenic D'Ambrosio*[⋆] *and Giorgio Guglieri*[⋆]
[⋆] *Department of Mechanical and Aereospace Engineering, Politecnico di Torino, Torino, Italy*
[♮] *MAVTech S.r.l., Torino, Italy*
nicoletta.bloise@polito.it · manuel.carreno@polito.it · erika.mai@mavtech.eu ·
domenic.dambrosio@polito.it · giorgio.guglieri@polito.it
[†]Corresponding author

Abstract

In recent years, developments in agriculture mechanization have generated relevant engineering challenges toward sustainable approaches. The introduction of the Unmanned Aircraft System (UAS) is continuously growing in several agricultural operations, such as precision spraying applications of Plant Protection Products (PPP). This work presents the design of a UAS with a dedicated spray system aiming to reduce the spray drift and enhance the efficiency of the operation in vineyards. For this purpose, we performed a numerical and experimental campaign to address the spray drift problem in the wake of a UAS. Conclusions from these activities allowed us to define restrictions and guidelines for UAS sprayers design. We propose a geometry and main characteristics of a hexacopter with an integrated spray system. Finally, we developed a wind estimation method to model an adaptive guidance algorithm that accounts for the spray drift.

1. Introduction

Now more than ever, the agricultural sector has a growing responsibility connected with global demographic growth and the rise in food production requirements. In particular, in recent years, the concept of Precision Agriculture (PA) has become increasingly important, thanks to the fourth agricultural revolution and the progress of technology. Regarding environment protection, PA focuses on the reduced availability of natural resources and the causes of resistance to chemical products. Especially with the rise of agricultural machines cause the pollution level tends to increase. Therefore, the optimization of farming operations is crucial. In parallel, the technological evolution of farm machinery and communication systems allows for an increase in the automation level in complex environments within sustainable agriculture, as discussed in [1, 2].

Unmanned Aerial Systems (UASs) combine with conventional machines, helicopters or human operators for certain automatic operations. In [3], the authors provide a detailed review of UAS applications for precision agriculture. Several aspects and technologies for different systems and payloads are studied in-depth, concentrating on aerial crop monitoring and spraying operations. In particular, the paper focuses on analyzing a spray system integrated on a UAS and its relative spray field under the rotor wake to evaluate the best operational parameters to carry out precision crop-spraying in vineyards. A preliminary design of this concept of rotary-wing UASS is shown by the authors in [4].

In particular, for three decades, aerial spray operations with UAS have been growing in some Asian countries, starting from Japan, expanding into South Korea and China [5] and nowadays, worldwide. Regarding high accessibility and popularity, the first research activities occurred in Asia in flat rice and corn canopies, where uniform distribution and good penetration are more critical than precision coverage. Since the advent of agricultural spraying, a crucial challenge has always been the drift problem (i.e. the sprayed pesticides that miss the target) that is becoming very important to evaluate the risk assessment of pesticide processes. Many studies have explored several factors that influence this phenomenon, including flight altitude and speed, nozzle type and geometry, spray pressure and wind speed, as in [6, 7, 8, 9]. Reference [10] shows an extension to a static configuration where the authors presented results of a UASS adapt control law by changing weather conditions to guarantee a precise pesticide deposition. The real difficulties are related to a more accurate request in terms of droplet position arising with 3D crops, usually placed in rows, such as orchard trees. For this canopy, the risk of off-target losses increases, and it is even more interesting to investigate the influence of the flight and spray parameters to obtain the required pesticide distribution and penetration on the canopy for different crops, as shown in [11, 12, 13, 14]. Optimal spray management in vineyards is of interest

DOI: 10.13009/EUCASS2022-6140

as these can present a sloped and irregular terrain and arrange in long narrow rows, as discussed in [15]. These characteristics create several challenges resulting in more complex precision spraying, and the flight mode becomes crucial to limit the drift towards the inter-row region. However, the limited payload availability makes the UASS advantageous only in critical areas difficult to reach by other machines and therefore, human operators are required. Therefore, our goal is to optimize spray deposition on the canopy and reduce waste of PPP, soil pollution and possibly human exposure to hazardous products.

The interaction between spray and rotors has been experimentally tested both in open field [16] and in wind tunnel facilities [17]. In parallel with experiments, numerical simulations to investigate the downwash flow field of multi-rotors have been performed. A lattice Boltzmann approach has been used in [18] to study the wake behind a plant protection hexacopter. Other computational models also include the study of droplet trajectories modelled using a Dispersed Phase Model (DPM) as shown in [19, 20, 21]. The authors show in [22] a similar approach by injecting Lagrangian particles in the wake of a hexacopter. We describe how the Lagrangian particle model requires injection inputs, such as droplet diameter, momentum and spray angle. These quantities are a priory unknown and difficult to predict accurately.

An adaptive guidance algorithm is required to limit the PPP off-target deposition, reducing the environmental impact of the spraying operations in vineyards. The atmospheric wind is one of the main factors that affect the targeting precision. Therefore, a real-time wind estimation strategy is necessary. This study presents a data-driven wind model only using data from the onboard sensors. Starting from the dynamical model of the multi-rotor and considering its control strategy, the UAS positions are correlated to the wind effects, allowing the extraction of wind magnitude and direction. This method was tested in-field, as discussed in [23] and in simulation showing satisfactory reliability, even though the vertical wind component is not studied. The tilt angle approach proposed in [23] can provide wind measurements only in hovering conditions. However, we resolve the problem using a correction based on the accelerometer measurements, as suggested in [24]. The paper shows a simple linear path planning above the rows of the vineyards to demonstrate the validity of the algorithm. The UAS trajectory is modified perpendicularly to the rows, using the model predictions to compensate for the sideways drift. On the other hand, the longitudinal drift is corrected by retarding or advancing in time the nozzle opening. Mixing in-field orographic and geometric analyses with a model of the PPP volume distribution, we obtain an estimation of the product deposited on the plant crown. The adaptive path planning accomplishes a more precise plant targeting, reducing the PPP environmental hazard and waste.

In this paper, we present the analysis and design of a UASS, aiming for the minimization of spray drift and versatility under different operation conditions. For this purpose, we present the results of an experimental and numerical campaign, partially anticipated in [22], where we studied the drift problem in a Wind Tunnel facility. The conclusions from these campaigns are used as inputs for the UASS design considerations. We define several restrictions concerning normative and UAS operation. The vineyard scenario is analyzed, focusing on the different operation modes and defining the Plant Protection Products (PPP) requirements. We also describe a dedicated adaptive control algorithm which can correct the UASS trajectory based on local wind estimation to minimize the spray drift.

This paper is organized as follows. In Section 2, an overview of the use of UASs for spray application on the vineyard is proposed. Section 3 describes how we have deepened the field of the interaction of the spray with rotors, experimentally and numerically. In addition, some significant results of this part are inserted. In Section 4, the design of UASS with some operational requirements for our mission are described. Then, to reduce the PPP environmental hazard and waste, an adaptive guidance algorithm that takes to account a real-time wind estimation is proposed in Section 5. Finally, our conclusions are drawn in Section 6.

2. Overview of UAS spray operation on vineyard

Our research proposes the introduction of the UAS in critical areas to perform spray precision operations. In the present study, the reference scenario is the vineyard. It is a challenging application to evaluate the efficiency of precision spraying due to the sloped terrain, muddy soils, and irregular narrow rows. In Figure 1, a graphical representation is used to explain the concept of spray application mode designed for our application, keeping the realistic dimensions of the vehicle and the vineyard (approximating a $2m$ row distance and a $0.5m$ row width). In particular, the UAS overflights of the vineyard row, spraying with two nozzles under the rotors to exploit the downwash of rotors 1 and 4. The average axial velocity induced by the rotors is around $10m/s$, and, therefore, spray droplets can be carried within the airflow and maximize the spraying over the plants, as shown in [20].

These hypotheses will be tested by CFD simulation and laboratory tests described below. We varied some parameters, such as vertical and radial nozzles position, altitude and flight speed, type of nozzles, and spray system pump pressure, to define the optimal operational parameters.

DOI: 10.13009/EUCASS2022-6140

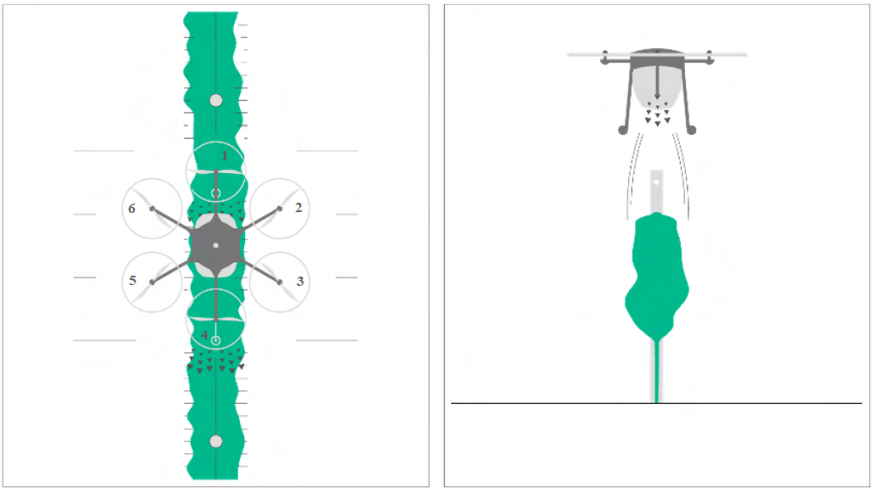

Figure 1: Spraying UAS flight mode on vine rows

3. Spray rotors interactions

In this section, we describe the methodology used to deepen the knowledge about the spray rotors' interactions. Starting from experimental testing in the wind tunnel, their results are compared with the CFD numerical to validate the numerical approach.

3.1 Wind tunnel test campaign

For the wind tunnel test campaign, we were hosted by the SEASTAR (Sustainable Energy Applied Sciences, Technology, and Advanced Research) at the Environment Park in Turin, Italy. In [22], more details of the wind tunnel testing (shown in Figure 2) are included.

Figure 2: UAS fixed in the SEASTAR Wind Tunnel

DOI: 10.13009/EUCASS2022-6140

3.1.1 Methodology

To obtain the desired results, flow visualization is performed employing LED illumination methodology with a high output of luminous flux of $4500lm$. The light source, is positioned to shoot backlighting photos obtaining a qualitative analysis of droplet distribution, as illustrated in Figure 3. Lateral and frontal photos are taken from a Nikon D750 that has a resolution of $6016x4016pixels$.

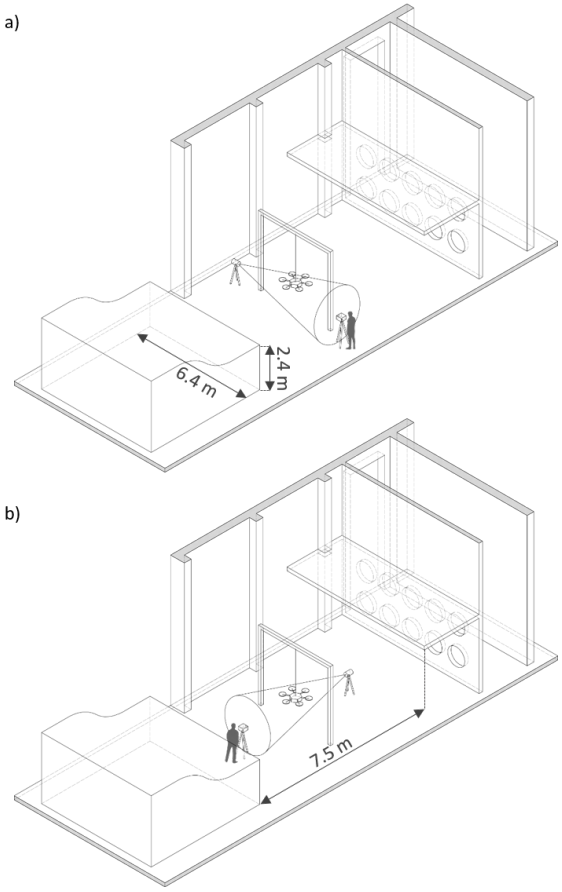

Figure 3: Spray visualization with LED technology in the Wind Tunnel: a) lateral view and b) frontal view

3.1.2 Data analysis

The automated process with which the images were analyzed allows us to extract relevant data from these and is divided into three phases:

- the RGB photos are converted, first into grayscale images and then filtered to obtain binary images, as shown in Figure 4, by applying an intensity threshold. This threshold is low as the light reflected from the droplets is faint.
- the binary image is block-processed, as shown in Figures 4. They are divided into small squares, and the number of white pixels that correspond to droplets is counted. To eliminate stray droplets, if the percentage of these white pixels is greater than a fixed threshold, the pixel concerned is considered to be part of the spray cone. Otherwise, it is discarded and completely coloured in black. Therefore, all points needed for the trajectory fitting are determined. Then, the images are divided into several horizontal rows, and the right and leftmost white pixels of each row are memorized as the limits of the spray cone. The process is repeated in columns. The pixels which verify both conditions are considered to be in the contour.
- a polynomial fitting of the contour points is performed approximating the spray shape, as shown in Figures 4 3).

DOI: 10.13009/EUCASS2022-6140

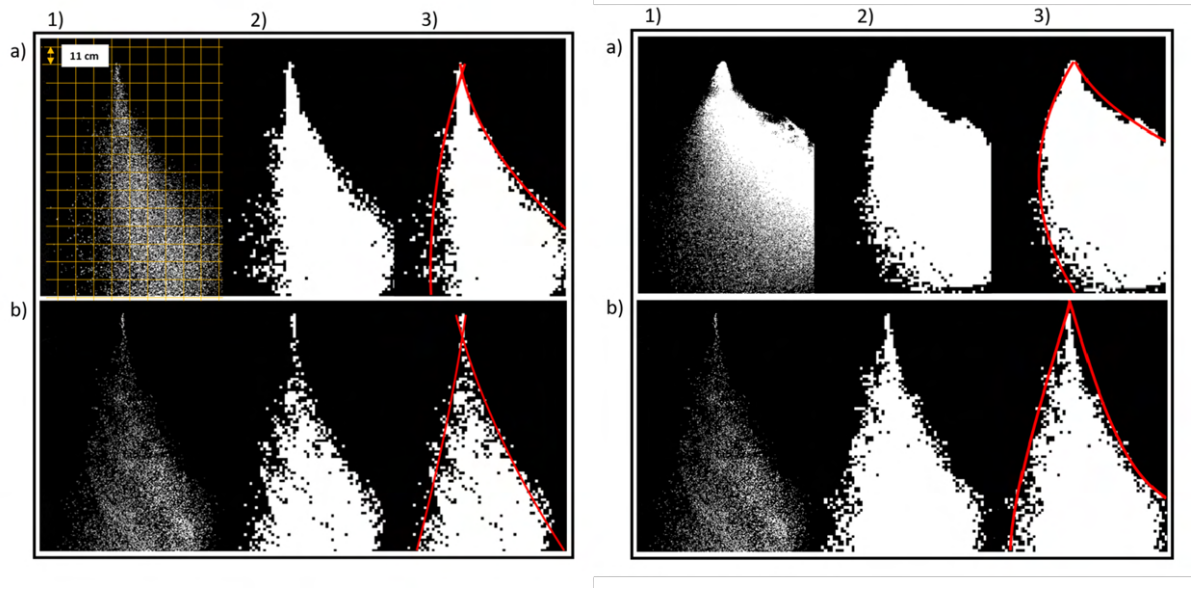

Figure 4: Spray with fan (left) and hollowcone (right) nozzles at $V = 2m/s$ a)$RPM = 1590$, b) $RPM = 5100$

3.2 CFD simulations

3.2.1 Numerical methods

The numerical model used to simulate the flow inside the wind tunnel is the segregated solver of the Unsteady Reynolds-Averaged Navier Stokes (URANS) equations embedded in the commercial CFD software STARCCM+ [25]. The turbulence model used is the one-equation Spalart-Almaras model [26]. The calculation of inviscid fluxes adopts a second-order reconstruction scheme combined with Roe's scheme, whereas the evaluation of viscous fluxes uses a second-order central difference. We performed numerical simulations using second order implicit time integration. The rotational motion of the rotors is modelled with a dynamic mesh approach in which a portion of the grid embedding the rotor slides inside an outer static grid using an Arbitrary Mesh Interface (AMI) protocol. This approach has been validated in [27, 28]. The flow in the wind tunnel is driven by ten fans, as shown in Figure 3. These are modelled with a fan type interface which assumes a finite pressure jump across a zero-thickness disk. The pressure jump is computed based on the fan performance curved supplied by manufacturers. The performance curve can be adjusted for different operating rotational velocities of the fans, which allows the adjustment of the velocity magnitude in the test section of the wind tunnel. The usual linear scaling for flow rate and quadratic scaling for pressure jumps, predicted by actuator disk theory, are used as shown in Equations 1 and 2. Figure 5 shows the velocity field inside the wind tunnel driven by the fans, including the UASS operating at $5100rpm$.

$$\Delta P_2 = \Delta P_1 \frac{\Omega_2^2}{\Omega_1^2} \tag{1}$$

$$V_2 = V_1 \frac{\Omega_2}{\Omega_1} \tag{2}$$

The spray droplets injected in our simulations are modelled with Lagrangian spherical particles. The linear momentum conservation law, shown in Equation 3, is solved.

$$m_p \frac{\mathbf{v}_p}{dt} = \mathbf{F}_g + \mathbf{F}_{vm} + \mathbf{F}_d + \mathbf{F}_p + \mathbf{F}_{sl} \tag{3}$$

where the forces acting on the particle are, from left to right, the gravity force, the virtual mass force, the drag force, the pressure gradient force and the shear lift force. The drag coefficient proposed in [29] has been used to compute the drag force. For the calculation of the shear lift, the expression provided in [30] has been employed.

The initial conditions for the integration of the conservation laws have been computed using a high-resolution interface capturing Volume Of Fluid (VOF) method in a separate CFD simulation of the employed nozzle. This methodology has been followed by [31, 32] among others to compute spray characteristics. This approach solves an extra scalar transport equation for the volume fraction as shown in Equation 4.

DOI: 10.13009/EUCASS2022-6140

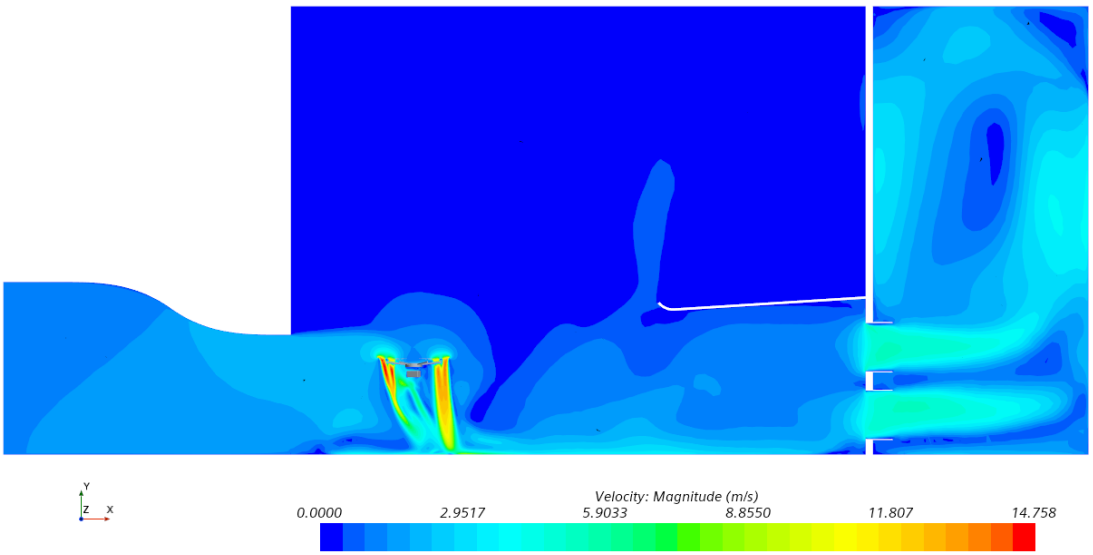

Figure 5: Instantaneous velocity magnitude field inside the wind tunnel operating at 2m/s and rotors operating at 5100RPM

$$\frac{\partial \alpha}{\partial t} + \nabla \cdot (\alpha \mathbf{u}) = 0 \tag{4}$$

The volume fraction is an indicator function which defines the phase. A value of 1 corresponds with "phase 1" (water), and a value of 0 corresponds with "phase 2" (air). The interphase can be defined with a value of the volume fraction of 0.5. The cells present in the interface region have to be refined in order to capture a sharp interphase. For this purpose, an Adaptive Mesh Refinement (AMR) strategy has been implemented to capture adequately the water-air interphase without the necessity of refining the whole computational domain. The Continuum Surface Force (CSF) approach, first described by Brackbill [33], is included to model the surface tension, which is known to be necessary to reproduce adequately the atomization process [34]. In order to avoid interphase blurring, the Courant Friedrich Levy (CFL) number has to be maintained below 1 even for implicit time integration schemes. In addition, to avoid this restrictive condition on the time step, a multi-stepping approach for the volume fraction transport equation has been used, allowing the global CFL condition to be relaxed, reducing in this way the computational cost of the simulations.

3.3 Pressure-Swirl Atomizers

The hollowcone nozzle used in the experimental campaign is provided by ARAG Group with the reference code HCI8002. This nozzle is classified as a pressure-swirl nozzle as a conical sheet of fluid is formed at the nozzle exit due to the centrifugal forces actuating in the rotating fluid inside the swirl chamber. The breakdown of the conical sheet first into ligaments and then into droplets is a very complex physical process which is extremely complex and expensive to model numerically [34]. Several authors, such as [32, 31] have employed interface capturing methods to resolve the conical sheet formation and even the ligament and particle breakdown. Four main characteristics define a hollowcone spray: i) particle diameter distribution, ii) film velocity, iii) film thickness and iv) cone angle. These parameters are strongly influenced by the injection pressure/mass flow and the nozzle geometry, especially by the exit orifice. The determination of the hollowcone spray characteristics is mandatory to model the interaction between the rotors and the spray. A simplified CAD model of the nozzle is shown in Figure 6.

This model represents the inner geometry of the nozzle and has been developed to allow an accurate CFD modelling of the multiphase flow. This nozzle is composed of three tangential inlets that make the flow rotate around the vertical axis in the so-called swirl chamber. The centrifugal forces push the fluid towards the wall, generating an air core inside the nozzle. This rotating liquid film is forced through the orifice, and the centrifugal forces make the liquid film expand, forming a conical fluid film.

DOI: 10.13009/EUCASS2022-6140

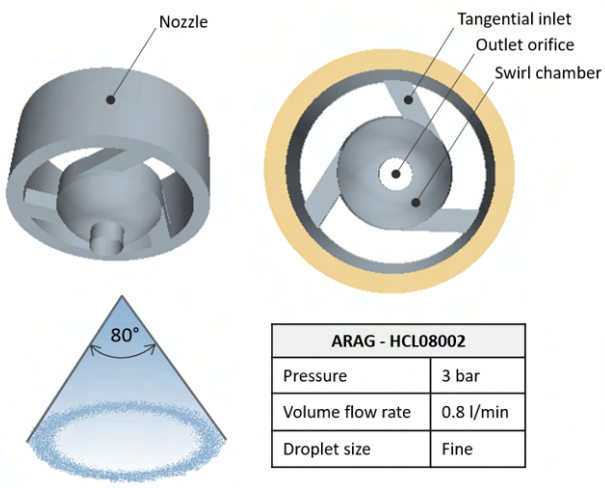

ARAG - HCL08002	
Pressure	3 bar
Volume flow rate	0.8 l/min
Droplet size	Fine

Figure 6: CAD model and some parameters of the HCI8002 nozzle

3.3.1 Droplet diameter distribution

The particle diameter distribution has been provided by the nozzle manufacturers for several pressures. We extrapolated the particle diameter distribution to our working pressure of 2 *bar* using a 3 point based Akima algorithm [35] for each droplet diameter. We can appreciate how the particle diameter approximates a log-normal distribution with parameters $\mu = 5.11$ and $\sigma = 0.52$.

3.3.2 Cone angle

Our visualization technique described in Section 3.1.1 allows the experimental determination of the outer angle of the conical sheet of liquid which becomes unstable and breaks down initially into ligaments and then into droplets [32]. Frontal images are used to measure the cone angle as shown in Figure 7. We can appreciate an angle of approximately 79° found in the experimental campaign.

Figure 7 shows the water-air interphase, which clearly shows a hollowcone shape, and this value agrees well with the cone angle found in the CFD simulation where a half cone angle of 40° is measured.

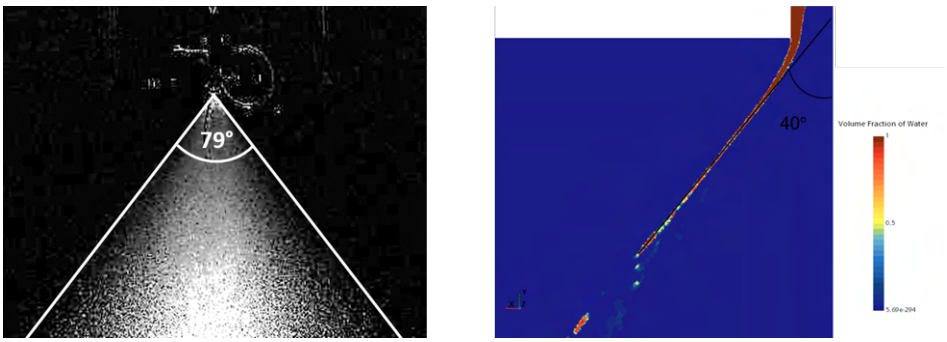

Figure 7: Hollowcone angle for a pressure of 2 bar measured during the experimental campaign(Left) and in CFD simulations(Right)

3.3.3 Film velocity and tangential velocity

As the number of droplets recovered in the numerical simulation is not enough to compute statistics on the velocity distribution of the particles and the correlation that can be found with the diameter, as shown in [6], we will assume that the droplets have a constant velocity equal to the film velocity. The film velocity is the non-tangential velocity component of the liquid contained in the conical sheet. Considering a cylindrical coordinate system (r, θ, z) centred on the exit orifice and with the z-axis coincident with the vertical axis, the film velocity (U_f) would be the result of combining the radial (U_r) and axial (U_z) components of velocity as shown in Equation 5.

DOI: 10.13009/EUCASS2022-6140

$$U_f = \sqrt{U_r^2 + U_z^2} \tag{5}$$

The film velocity presents a constant value before the instabilities trigger the breakdown of the conical sheet. Even though there are not sufficient droplets to consider statistical convergence, most of the droplets present a very close value comprised between 14 and $15 m/s$ and therefore selecting a constant value of the injection velocity of the particles is justified.

On the other hand, the tangential velocity (U_θ) is not constant as the fluid film evolves and decreases as the radial coordinate of the cone increases. We noticed that at the end of the simulated region, the tangential velocity is close to zero, and therefore, we are going to simulate Lagrangian particles without an initial tangential velocity.

3.4 Wind effects on the hollow cone spray

Simulations using the 80° cone angle for the injection of Lagrangian particles reveal much wider droplet dispersion compared to the experimental measurements, suggesting that the conical sheet is being deformed before droplets detach from the ligaments and hence the effective injection angle of the Lagrangian particles is modified. In an attempt to capture first order effects of the rotor downwash on the droplet formation, a multiphase simulation was performed with a constant vertical wind. From the simulation of the hexacopter for the case of a maximum throttle, the induced velocity at the injection point equal to $12 m/s$ is used. Figure 8 shows a significant closure of the cone angle from 80° to 56°. The angle of 56° was used in the hollowcone injector of Lagrangian particles.

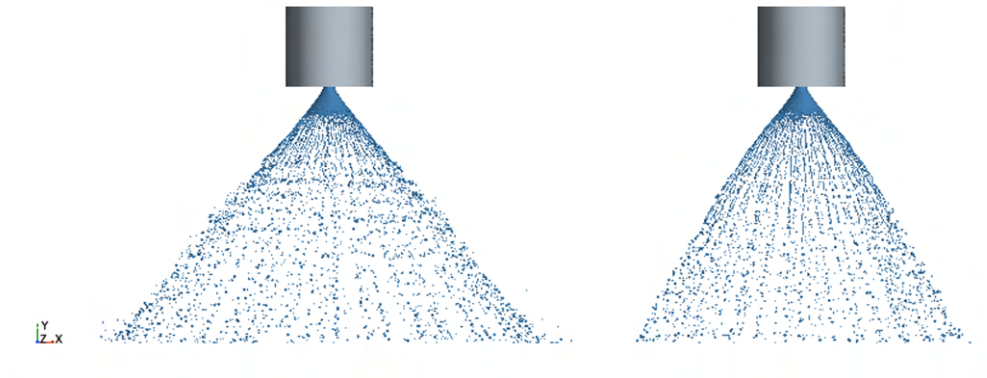

Figure 8: Water-air interphase in VOF CFD simulation showing the conical sheet of fluid produced by the pressure swirl nozzle at a pressure of 2 *bar* with no axial velocity (left) and with axial velocity of 12 m/s (right)

3.5 Experimental Validation

The previous sections explained how we have estimated the initial conditions (momentum, diameter and cone angle) for the Lagrangian particle injection model. The mass flow rate has been set to a value of 0.67 litres per second, as in the VOF simulation. A random number generator following a lognormal distribution with $\mu = 5.11$ and $\sigma = 0.52$ has been employed to inject particles with diameters coherent with the statistical distribution extrapolated from manufacturers' data. Particles are injected during 2 seconds to allow converged statistics and to give time for them to be convected by the flow.

To assess the validity of the developed numerical model, we present a comparison between experimental LED visualization images and the distribution of Lagrangian particles. We have performed this validation with the wind tunnel operating at $2 m/s$ and the rotor operating at full throttle. The comparison is shown in Figure 9. We can appreciate how the lateral views are congruent, presenting similar cone angles, and the lateral wind-induced drift is evident. A slight deviation towards the left is also appreciable , comparing our Lagrangian particles with droplet visualization. This is possibly due to the fact that in Section 3.4 a fully vertical flow was considered, and indeed a small component of cross-flow would be present that could eventually deform the hollowcone fluid sheet slightly modifying injection parameters. Another possible source of error is a slight misalignment of the injector in the experimental campaign caused by the impulsive activation of the spray system. CFD simulations give additional information as we can track every particle in the 3-dimensional domain. In addition, it is appreciated how the drift is extremely sensitive to particle diameter. Large particles (red and orange) maintain considerably well the conical sheet structure due to their

DOI: 10.13009/EUCASS2022-6140

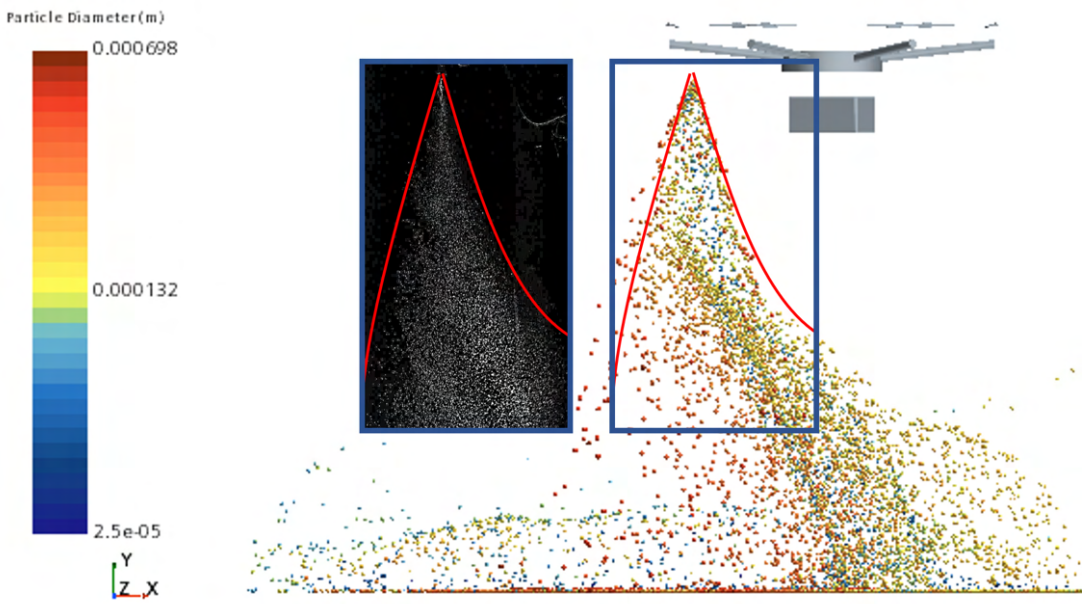

Figure 9: Comparison between droplet LED visualization and CFD simulations with rotors at full throttle and a wind speed of 2 m/s.

large inertia, which makes them much less sensitive to the velocity and pressure fields. On the other hand, the smaller particles (yellow, green and blue) are affected by the flow, which convects the droplets upstream and downstream of the hexacopter. However, we appreciate how most of the particles are contained in the wake and how this directs the particles towards the ground, reducing drift. To show the beneficial effect of the rotor downwash, Figure 10 shows the comparison of the droplet distributions obtained with and without the rotors operating at full speed. The drift is drastically minimized except for a lateral flow generated when the particles leave the downwash region. The use of smaller cone aperture angles could be useful to reduce this drift, allowing the droplets to be contained in the high velocity wake region until they are very close to the ground. It is worth mentioning that small particles ($<100\mu m$) represent a small volume fraction of the sprayed liquid due to the cubic relationship between diameter and volume. Another illustrative result is how, when rotors are off, the particle distribution becomes stratified by diameters.

4. Design of an hexacopter for spraying application

In this section, following experimental testing and numerical simulation suggestions, we dealt with the UAS design and drew up a list of operational requirements.

4.1 Design of UASS

Initially, we carried out a trade-off and a market analysis comparing quadrotors and hexacopters before proceeding with the design. The solution with six rotors for this type of mission and size is considered the best choice for several reasons, particularly for reducing the problem of structural vibrations during the flight. In Europe, EASA works to keep up with the exponential development that has taken place in the civil sector in recent years and streamlining the regulations to facilitate research and development of the new autonomous system, as authors discuss in [36] specifically for the agriculture applications. To remain in the *open* category, which does not require any prior operational authorization and declaration by the UAS operator, the Maximum Take-Off Weight (MTOW) must be less than 25 kg. However, a more restrictive constraint consists of continuous Visual Line Of Sight (VLOS) remote piloting to guarantee a safe flight.

The first phase of design concerns the propulsion system to ensure a thrust-to-weight ratio greater than 2. We opted for motors, ECS and propellers of T-Motor and LiPo Battery of Tattu. The span of the drone is about $1.75m$, measuring from tip to tip of diagonal rotors. Our CAD is shown in Figure 11.

DOI: 10.13009/EUCASS2022-6140

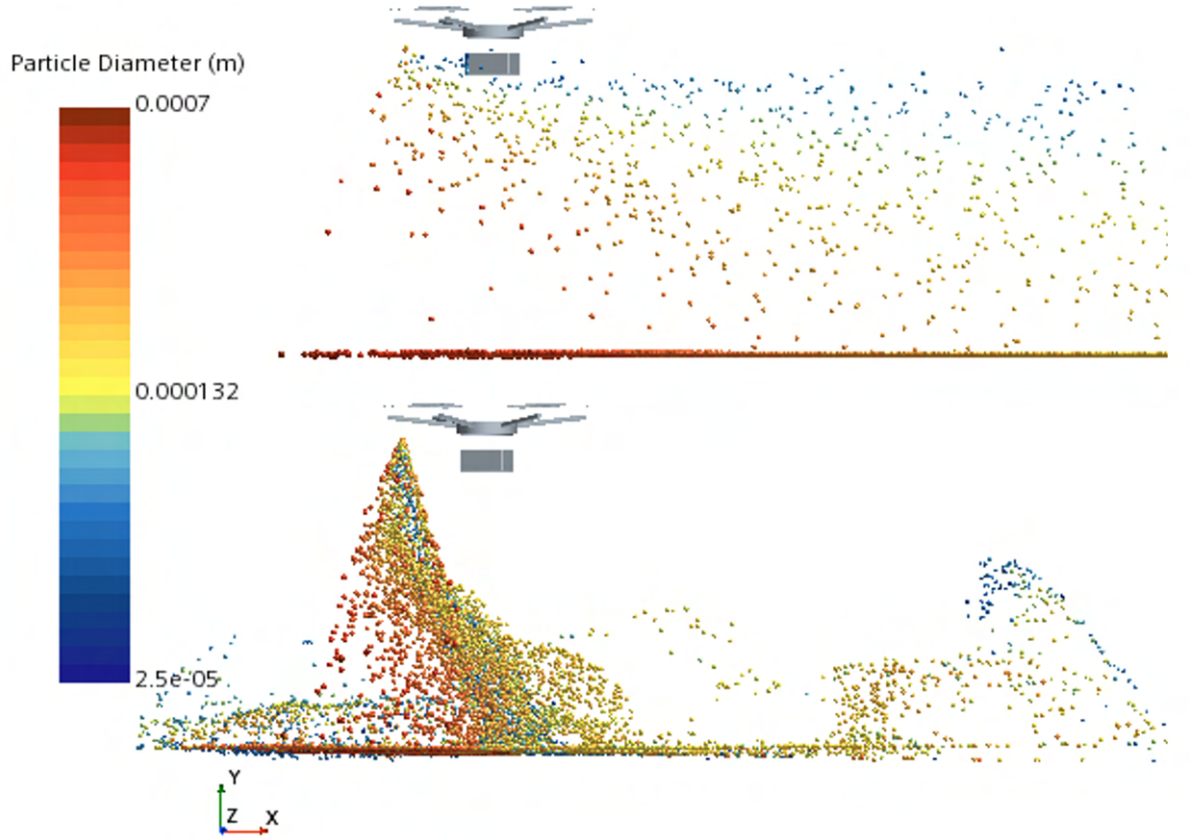

Figure 10: Comparison between CFD simulations with a wind speed of 2 m/s with rotors off (top) and rotors at full throttle (bottom)

A critical consideration of the weight distribution is that the average PPP flow rate should be around $2.4L/min$. Considering the capacity of the tank of 10L, in a little over 4 minutes, the UAS needs to land and refill. Therefore, compared to the classic 30% of the MTOW dedicated to the payload, for this project, we assigned 50% of the entire spray system, including the tank, jeopardizing the battery and then the endurance.

4.2 Operational requirements

From previous studies and our results than previously shown, we have compiled a list of operational requirements for a successful spraying mission on the vineyard.

The flight altitude is fixed at around $2 - 2.5m$ above the ground to be approximately half a meter above the plant. To permit an adequate droplet penetration inside the plants and to avoid the horseshoe vortices, the forward velocities must remain within the range of $1.5 - 3m/s$. Moreover, the UAS controller shall be able to manage a wind speed up to $3m/s$. Above this value, the mission should be suspended. Regarding the spray system requirements, front and back nozzles shall be placed under the rotors to exploit the downwash, as shown in figures 10 and 4. In addition, to spray only on the plant, the best nozzle is the hollow cone ceramic with a spray cone of $40 - 60$ °. The nozzle diameter and the system's pressure depend on the flow rate required by the agronomists. Preliminary field tests show that at least $2.4L/min$ is necessary for UAS spraying operations on vineyards.

4.3 Spray system

Our spraying UAS has to be equipped with a standalone spray system able to switch on and off nozzles depending on the mission type. Another important factor that influences the dimension of the droplets is the nozzle operation pressure, and therefore a pressure regulator is included to set the pressure in the optimal range defined by the nozzle manufacturers to obtain precise droplet size, as suggested in [7].

DOI: 10.13009/EUCASS2022-6140

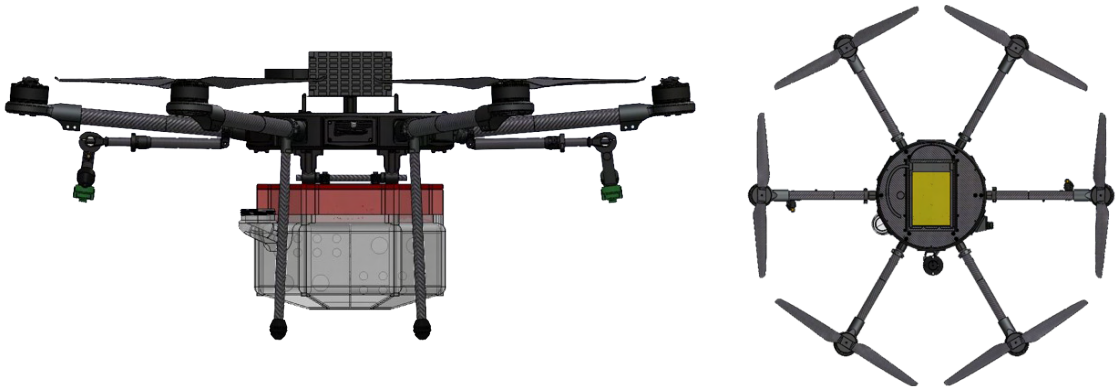

Figure 11: Lateral (left) and Top (right) view of the CAD of our spraying UAS design

In detail, the circuit of the spray system is reported in 12. An external battery 4S (1800mAh) powers a membrane pump (Cybernova Pump, 70 W power) able to generate a maximum flow rate of 6L/min that can switch on/off spray operations by a radio remote control. As mentioned before, downstream of the pump, there is a manual pressure regulator (with a maximum flow rate of 20 L/min) and then a vacuum pressure gauge (measuring range of 0-0.6 MPa) to measure the pressure level in real-time. Finally, two nozzles are defined to guarantee the correct liquid flow rate. For this mission on the vineyard, to respect the requests of agronomists, the guaranteed range must be between 1.2

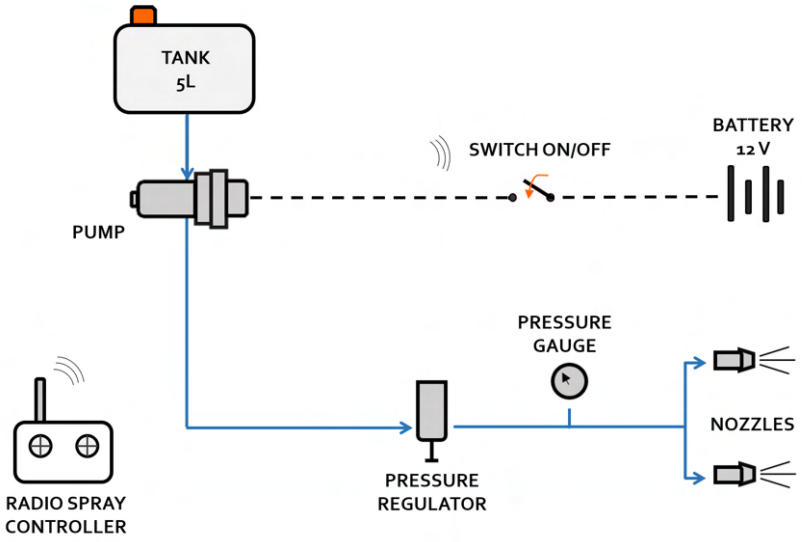

Figure 12: Spray system circuit

and 2.4L/min, and therefore, the spray pressure must be fixed at 0.3MPa according to the nozzle size (ISO 015 and ISO 02). Finally, an adequate tank design is fundamental to reducing the nonlinear oscillatory movement of the liquid inside as much as possible, as previously discussed in [37, 38]. We investigated and analyzed different tank shapes with and without baffles in numerical simulation, hypothesizing characteristic accelerations of the UAS dynamics. As shown in Figure 11, a customized tank dedicated is designed for 10L with a hexagonal geometry and perforated plates inside to minimize the sloshing phenomenon. The size of the tank is the same as the frame that contains the electronics of the drone, and above this, there is a box that contains the other components of the spray system.

5. Adaptive path planning in windy environments

An adaptive path planning is essential to perform practical operations in the field, to approach sustainable agriculture and, in particular, to minimize the PPP drift. The atmospheric wind is the main factor that affects the targeting precision. It should be considered in the mission planning and execution, exploiting it to deposit the protection products only

DOI: 10.13009/EUCASS2022-6140

where needed. This section describes how the guidance algorithm uses droplets' trajectory and wind estimation to correct the path planning.

Initially, a wind estimator algorithm is implemented to know the wind magnitude and direction to evaluate the spray footprint centre in real-time by the model previously described through experimental and numerical curves. Many pieces of research have been focused on wind estimation using UAS. Some of them consist of onboard sensors that directly measure airspeed, although indirect measurement strategies are present in literature, as presented in [23]. Once a robust wind estimation is available onboard, it is possible to develop a correction algorithm that takes into account these sensors' data to minimize the drift problem. The correction is achieved in two different ways

- the first one directly acts on the vehicle position by modifying the *path plan* and moving the UAS laterally to the length of vine rows.
- The second one controls the particles' deposition by turning on and off the spray circuit when needed. Based on the spray model, the system can predict where the particles will deposit: if the deposition area overlaps the target zone, the nozzle opens. Otherwise, it shuts off.

This strategy is needed because, if the correction is achieved only by controlling the position, any sudden wind change in the longitudinal direction (concerning the row's length) makes the vehicle swing back and forth. This motion will cause over-spraying of the underlying plants, reducing the overall accuracy distribution.

The case study consists of linear straight passes above the rows on a flat vineyard. The rows are assumed to be 20 m long, and the product distribution aims to be homogeneous on all plants.

5.1 Simulations

We present some significant results of the simulations in the previously described scenario. A six-degree-of-freedom (DOF) UAS rigid body model with the adaptive guidance algorithm and Proportional-Integrative-Derivative (PID) controller is implemented in a MATLAB/Simulink environment. Observing PPP droplet distribution in Figure 13, it becomes evident how this logic improves the system accuracy (the product is deposited on the plants). In contrast, when the path correction algorithm is deactivated, the deposition is severely degraded and rarely targets the vineyard rows.

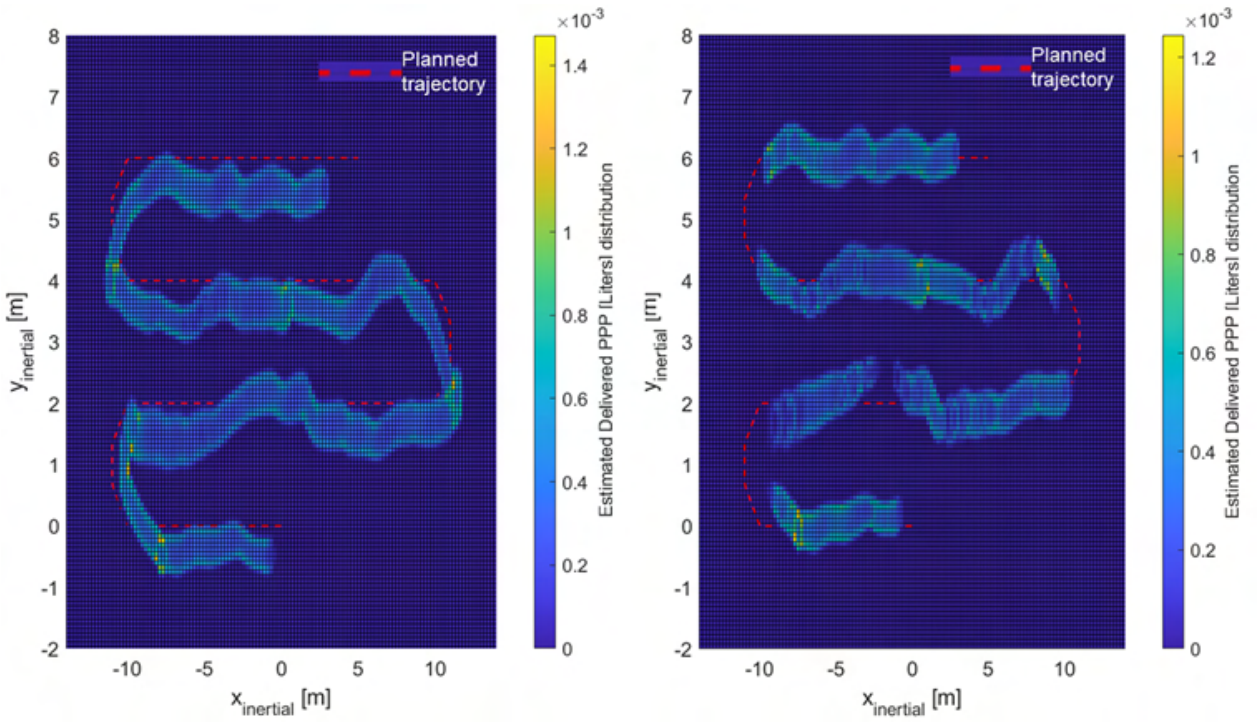

Figure 13: PPP plant distribution without and with spray adaptive control system

DOI: 10.13009/EUCASS2022-6140

6. Conclusions

To accomplish the ambitious challenge of reducing the off-target deposition of PPP, we propose a drone design with an MTOW equal to 25kg that includes a dedicated spray system for aerial spray application with an anti-sloshing tank. The design allows a variable nozzle position that is necessary as the optimal position depends on the operation conditions. The optimal flight mode and operational parameters, the position and type of the nozzle, the flow pressure, and an adaptive guidance algorithm have been defined after performing experimental testing and CFD simulations. The numerical model has been compared with the experimental results showing satisfactory agreement. Both reveal that placing the nozzles below the rotors constitutes an advantage for drift reduction. Large velocities produce a significant spray drift, which reduces the efficiency of the operation and also increases the mass flow requirements of the spray system. This will require a larger pump and an increase in weight of the UAS. The inclusion of an adaptive path planning increases the efficiency of the spray by allowing the UAS to fly not directly above the vine rows in such a way that the spray deposition on the plants is maximized.

The next step is to simulate in CFD analysis this new UAS with the spray system to evaluate the droplet distribution and to integrate these results in the path planning, taking into account the adaptive algorithm and control system. Finally, the experimental testing in the field in a windy environment would be interesting to assess the performance of wind estimation and the improvement of target deposition.

Acknowledgment

This research was funded by the project “New technical and operative solutions for the use of drones in Agriculture 4.0” (Italian Ministry of University and Research - Progetti di Ricerca di Rilevante Interesse Nazionale – PRIN 2017, Prot. 2017S559BB).

The authors gratefully acknowledge the support and would like to thank MAVTech S.r.l. for the design and realization of structural and mechanical parts for the wind tunnel experimental testing.

References

[1] M. H. Saleem, J. Potgieter, and K. M. Arif, “Automation in agriculture by machine and deep learning techniques: A review of recent developments,” *Precision Agriculture*, vol. 22, no. 6, pp. 2053–2091, 2021.

[2] G. Idoje, T. Dagiuklas, and M. Iqbal, “Survey for smart farming technologies: Challenges and issues,” *Computers & Electrical Engineering*, vol. 92, p. 107104, 2021.

[3] P. Radoglou-Grammatikis, P. Sarigiannidis, T. Lagkas, and I. Moscholios, “A compilation of UAV applications for precision agriculture,” *Computer Networks*, vol. 172, p. 107148, 2020.

[4] N. Bloise, M. Carreño Ruiz, D. D’Ambrosio, and G. Guglieri, “Preliminary design of a remotely piloted aircraft system for crop-spraying on vineyards,” in *2020 IEEE International Workshop on Metrology for Agriculture and Forestry (MetroAgriFor)*. IEEE, 2020, pp. 1–6.

[5] X. He, “Rapid development of unmanned aerial vehicles (uav) for plant protection and application technology in china,” *Outlooks on Pest Management*, vol. 29, no. 4, pp. 162–167, 2018.

[6] D. Nuyttens, K. Baetens, M. De Schampheleire, and B. Sonck, “Effect of nozzle type, size and pressure on spray droplet characteristics,” *Biosystems engineering*, vol. 97, no. 3, pp. 333–345, 2007.

[7] S. Chen, Y. Lan, Z. Zhou, F. Ouyang, G. Wang, X. Huang, X. Deng, and S. Cheng, “Effect of droplet size parameters on droplet deposition and drift of aerial spraying by using plant protection uav,” *Agronomy*, vol. 10, no. 2, p. 195, 2020.

[8] F. Ahmad, B. Qiu, X. Dong, J. Ma, X. Huang, S. Ahmed, and F. A. Chandio, “Effect of operational parameters of uav sprayer on spray deposition pattern in target and off-target zones during outer field weed control application,” *Computers and Electronics in Agriculture*, vol. 172, p. 105350, 2020.

[9] G. Wang, Y. Han, X. Li, J. Andaloro, P. Chen, W. C. Hoffmann, X. Han, S. Chen, and Y. Lan, “Field evaluation of spray drift and environmental impact using an agricultural unmanned aerial vehicle (uav) sprayer,” *Science of the Total Environment*, vol. 737, p. 139793, 2020.

[10] B. S. Faiçal, H. Freitas, P. H. Gomes, L. Y. Mano, G. Pessin, A. C. de Carvalho, B. Krishnamachari, and J. Ueyama, "An adaptive approach for uav-based pesticide spraying in dynamic environments," *Computers and Electronics in Agriculture*, vol. 138, pp. 210–223, 2017.

[11] Y. Meng, J. Su, J. Song, W.-H. Chen, and Y. Lan, "Experimental evaluation of uav spraying for peach trees of different shapes: Effects of operational parameters on droplet distribution," *Computers and Electronics in Agriculture*, vol. 170, p. 105282, 2020.

[12] J. Martinez-Guanter, P. Agüera, J. Agüera, and M. Pérez-Ruiz, "Spray and economics assessment of a uav-based ultra-low-volume application in olive and citrus orchards," *Precision Agriculture*, vol. 21, no. 1, pp. 226–243, 2020.

[13] C. Wang, A. Herbst, A. Zeng, S. Wongsuk, B. Qiao, P. Qi, J. Bonds, V. Overbeck, Y. Yang, W. Gao *et al.*, "Assessment of spray deposition, drift and mass balance from unmanned aerial vehicle sprayer using an artificial vineyard," *Science of The Total Environment*, vol. 777, p. 146181, 2021.

[14] X. Li, D. K. Giles, F. J. Niederholzer, J. T. Andaloro, E. B. Lang, and L. J. Watson, "Evaluation of an unmanned aerial vehicle as a new method of pesticide application for almond crop protection," *Pest Management Science*, vol. 77, no. 1, pp. 527–537, 2021.

[15] D. Sarri, L. Martelloni, M. Rimediotti, R. Lisci, S. Lombardo, and M. Vieri, "Testing a multi-rotor unmanned aerial vehicle for spray application in high slope terraced vineyard," *Journal of Agricultural Engineering*, vol. 50, no. 1, pp. 38–47, 2019.

[16] Y. Zhan, P. Chen, W. Xu, S. Chen, Y. Han, Y. Lan, and G. Wang, "Influence of the downwash airflow distribution characteristics of a plant protection uav on spray deposit distribution," *Biosystems Engineering*, vol. 216, pp. 32–45, 2022.

[17] Q. Liu, S. Chen, G. Wang, and Y. Lan, "Drift evaluation of a quadrotor unmanned aerial vehicle (uav) sprayer: Effect of liquid pressure and wind speed on drift potential based on wind tunnel test," *Applied Sciences*, vol. 11, no. 16, p. 7258, 2021.

[18] H. Zhang, L. Qi, Y. Wu, E. M. Musiu, Z. Cheng, and P. Wang, "Numerical simulation of airflow field from a six–rotor plant protection drone using lattice boltzmann method," *Biosystems Engineering*, vol. 197, pp. 336–351, 2020.

[19] F. Yang, X. Xue, C. Cai, Z. Sun, and Q. Zhou, "Numerical simulation and analysis on spray drift movement of multirotor plant protection unmanned aerial vehicle," *Energies*, vol. 11, no. 9, p. 2399, 2018.

[20] S. Wen, J. Han, Z. Ning, Y. Lan, X. Yin, J. Zhang, and Y. Ge, "Numerical analysis and validation of spray distributions disturbed by quad-rotor drone wake at different flight speeds," *Computers and Electronics in Agriculture*, vol. 166, p. 105036, 2019.

[21] L. Wang, M. Xu, Q. Hou, Z. Wang, Y. Lan, and S. Wang, "Numerical verification on influence of multi-feature parameters to the downwash airflow field and operation effect of a six-rotor agricultural uav in flight," *Computers and Electronics in Agriculture*, vol. 190, p. 106425, 2021.

[22] N. Bloise, M. Carreño Ruiz, D. D'Ambrosio, and G. Guglieri, "Wind tunnel testing of remotely piloted aircraft systems for precision crop-spraying applications," in *2021 IEEE International Workshop on Metrology for Agriculture and Forestry (MetroAgriFor)*. IEEE, 2021, pp. 378–383.

[23] P. Abichandani, D. Lobo, G. Ford, D. Bucci, and M. Kam, "Wind measurement and simulation techniques in multi-rotor small unmanned aerial vehicles," *IEEE Access*, vol. 8, pp. 54 910–54 927, 2020.

[24] Y. Song, Q.-H. Meng, B. Luo, M. Zeng, S.-G. Ma, and P.-F. Qi, "A wind estimation method for quadrotors using inertial measurement units," in *2016 IEEE International Conference on Robotics and Biomimetics (ROBIO)*. IEEE, 2016.

[25] P. Siemens, "Star-ccm+ user guide version 14.06," *Siemens PLM software Inc*, 2019.

[26] P. Spalart and S. Allmaras, "A one-equation turbulence model for aerodynamic flows," in *30th Aerospace Sciences Meeting and Exhibit*. [Online]. Available: https://arc.aiaa.org/doi/abs/10.2514/6.1992-439

[27] M. Carreño Ruiz, M. Scanavino, D. D'Ambrosio, G. Guglieri, and A. Vilardi, "Experimental and numerical analysis of multicopter rotor aerodynamics," in *AIAA Aviation 2021 Forum*, 2021, p. 2539.

[28] M. Carreño Ruiz, A. Manavella, and D. D'Ambrosio, "Numerical and experimental validation and comparison of reduced order models for small scale rotor hovering performance prediction," in *AIAA SCITECH 2022 Forum*, 2022, p. 0154.

[29] L. Schiller, "Über die grundlegenden berechnungen bei der schwerkraftaufbereitung," *Z. Vereines Deutscher Inge.*, vol. 77, pp. 318–321, 1933.

[30] M. Sommerfeld, "Theoretical and experimental modelling of particulate flows," *VKI Lecture Series*, vol. 6, pp. 3–7, 2000.

[31] E. Laurila, J. Roenby, V. Maakala, P. Peltonen, H. Kahila, and V. Vuorinen, "Analysis of viscous fluid flow in a pressure-swirl atomizer using large-eddy simulation," *International Journal of Multiphase Flow*, vol. 113, pp. 371–388, 2019.

[32] M. Di Martino, D. Ahirwal, and P. L. Maffettone, "Three-dimensional computational fluid dynamics simulation of the hollow-cone spray process: The stability of the conical liquid sheet," *Physics of Fluids*, vol. 33, no. 6, p. 063301, 2021.

[33] J. U. Brackbill, D. B. Kothe, and C. Zemach, "A continuum method for modeling surface tension," *Journal of computational physics*, vol. 100, no. 2, pp. 335–354, 1992.

[34] A. H. Lefebvre and V. G. McDonell, *Atomization and sprays*. CRC press, 2017.

[35] H. Akima, "A new method of interpolation and smooth curve fitting based on local procedures," *Journal of the ACM (JACM)*, vol. 17, no. 4, pp. 589–602, 1970.

[36] J. del Cerro, C. Cruz Ulloa, A. Barrientos, and J. de León Rivas, "Unmanned aerial vehicles in agriculture: A survey," *Agronomy*, vol. 11, no. 2, p. 203, 2021.

[37] E. Frosina, A. Senatore, A. Andreozzi, F. Fortunato, and P. Giliberti, "Experimental and numerical analyses of the sloshing in a fuel tank," *Energies*, vol. 11, no. 3, p. 682, 2018.

[38] S. Ahmed, B. Qiu, F. Ahmad, C.-W. Kong, and H. Xin, "A state-of-the-art analysis of obstacle avoidance methods from the perspective of an agricultural sprayer uav's operation scenario," *Agronomy*, vol. 11, no. 6, p. 1069, 2021.